

Interplay between Yu-Shiba-Rusinov states and spin-flip excitations on magnetic impurities on superconducting NbSe₂ substrate

Shawulienė Kezilebieke,¹ Rok Žitko,^{2,3} Marc
Dvorak,¹ Teemu Ojanen,^{1,4} and Peter Liljeroth^{1,*}

¹*Department of Applied Physics, Aalto University School of Science, 00076 Aalto, Finland*

²*Jožef Stefan Institute, Jamova 39, SI-1001 Ljubljana, Slovenia*

³*Faculty of Mathematics and Physics, University of Ljubljana,
Jadranska 19, SI-1000 Ljubljana, Slovenia*

⁴*Laboratory of Physics, Tampere University of Technology, Tampere FI-33101, Finland*

(Dated: April 28, 2022)

Abstract

Exchange coupling between a magnetic impurity and a superconducting substrate results in the formation of Yu-Shiba-Rusinov (YSR) bound states, which have been recently used in artificial designer structures to realize exotic quasiparticles known as Majorana fermions. At strong coupling, the energies of YSR states are deep in the superconducting gap, and the impurity can even undergo a transition from high-spin to low-spin magnetic state by trapping one or several Bogoliubov quasiparticles from the bulk. At weak coupling, the YSR states migrate towards the superconducting gap edge. Additional spectral features can appear in the presence of magnetic anisotropy with spin $S \geq 1$, in particular spin-flip excitations outside the superconducting gap. Despite extensive experiments on magnetic impurities that exhibit separately either spin-flip excitations or YSR states, these phenomena have not been observed simultaneously. Here, we investigate the spectral evolution in different metal phthalocyanine molecules on NbSe₂ surface as a function of the coupling with the substrate. Using scanning tunneling microscopy (STM), we tune the exchange coupling strength and for manganese phthalocyanine (MnPc) we demonstrate a smooth spectral crossover from the YSR states to intrinsic quantum spin states. These results provide crucial insight into the fundamental behaviour of magnetic/superconducting hybrid systems and could have significant ramifications for the design and control of atomic scale magnetic devices.

Precise control of the properties of magnetic impurities on surfaces, such as the spin state and magnetic anisotropy, is one of the ultimate goals in fabricating atomic or molecular scale devices for data storage or computing purposes. However, the properties of magnetic impurities are strongly influenced by the atomic environment. In the extreme case, the interactions with the environment (substrate) can create entirely new electronic states, such as the Kondo effect on metallic substrates [1–3], or the formation of Yu-Shiba-Rusinov (YSR) bound states on superconductors [4–8]. Recently, YSR states have received intense interest as it has become possible to create artificial designer structures, where the interaction between the YSR states gives rise to Majorana modes [9–16]. The YSR states are very sensitive to the immediate environment of the impurity spin; therefore, YSR states can also be used to understand the role of the local environment on the exchange interaction J of an impurity spin with a superconductor [3, 7, 12, 15–22].

The bulk of recent experimental work on YSR states on superconducting (SC) substrates has demonstrated that the strength of the exchange interaction J can be significantly influenced by a small change in the adsorption site of the impurity or by spacers between the impurity and substrate [3, 18, 23–25]. While increasing J eventually induces a quantum phase transition to a reduced-spin ground state [3, 24, 26, 27], reducing J causes YSR states to migrate towards the SC gap edge. New symmetric features with respect to E_F , arising from inelastic spin-flip excitations, can appear outside the gap for $S \geq 1$ [18, 25, 28–33]. These two distinct phenomena - YSR states and spin-flip excitations - are illustrated in Fig. 1a and b.

High-spin systems are subject to the magnetocrystalline anisotropy, i.e., the dependence of the energy of the magnetic moment on its orientation relative to the atomic environment. It has been experimentally observed that exchange coupling strongly affects the anisotropy of an impurity coupled to an electronic bath [34]. However, despite extensive experimental and theoretical studies on both spin-flip excitations or YSR states in similar systems, the interplay and cross-over between spin-flip excitations and YSR states has not yet been demonstrated. Here we experimentally and theoretically investigate the spectral evolution arising from the competition between the YSR states and inelastic spin excitations in different spin systems of M–phthalocyanine molecules (MPc, where M: Co, Mn, Cu, Fe, Fig. 1c) on NbSe₂ surface. By using the scanning tunneling microscope (STM) tip, we can tune the exchange coupling strength J , and follow the spectral evolution from the YSR states

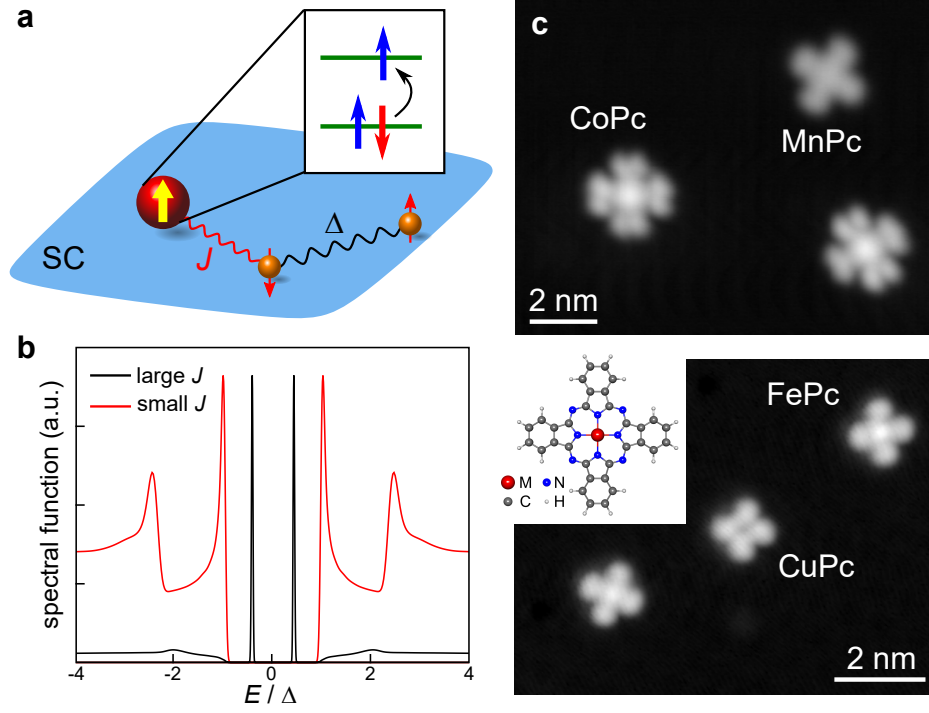


FIG. 1. **Paramagnetic impurity in contact with an s-wave superconductor.** **a**, Impurity spin is exchange coupled with strength J to the superconducting substrate (gap Δ). **b**, Impurity locally breaks the time-reversal symmetry and induces pairs of bound states symmetric with respect to E_F within the gap of the quasiparticle excitation spectrum (black curve). When J is reduced, the YSR states migrate close to the SC coherence peaks. For impurities with $S \geq 1$, the internal spin degrees of freedom can still result in symmetric features with respect to E_F outside the SC gap (red curve). **c**, Topographic STM images of the molecules used in this study (imaging set-point 0.5 V / 2 pA). Schematic of a MPc molecule is shown in the inset.

to intrinsic quantum spin states characterized by well-developed spin-flip excitations. Our experiments, combined with calculations, show that this is a smooth cross-over. The excitation energies furthermore reveal a significant renormalization of the anisotropy by the exchange coupling with the superconducting electrons and, in addition, the coupling has a strong effect on the excited spin lifetime. Our results provide detailed understanding of the low-energy quantum states in magnetic/superconducting hybrid systems and could have significant ramifications for the design and control of atomic-scale magnetic devices.

Figure 1a illustrates how the exchange coupling J with the substrate competes with the superconducting pairing energy Δ . The interaction of the local spin with the Cooper

pairs gives rise to a low-lying excited state within the gap of the quasiparticle excitation spectrum [4–8]. When J is decreased, the direct interaction of the local spin with the Cooper pairs is reduced and the YSR states merge with the SC coherence peaks. In the simplified theory of Yu, Shiba and Rusinov, the position of the YSR state is given by $E_{\text{YSR}} = \Delta(1-\alpha^2)/(1+\alpha^2)$ with α proportional to J , $\alpha = \pi\rho JS/2$, where ρ is the normal-state density of states of the substrate at the Fermi level and S is the impurity spin. The bound state results from the spin-dependent scattering of Bogoliubov quasiparticles on the impurity and is thus associated with the longitudinal part of the exchange interaction, $JS_z s_z$, where the lower-case s represents the spin-density of the substrate electrons at the position of the impurity. Furthermore, internal spin transitions in combination with magnetic anisotropy can give rise to symmetric features with respect to E_F outside the superconducting gap as shown in Fig. 1b. These are associated with the spin-flip events, whereby the spin projection changes by ± 1 [28, 32, 33]. The renormalization of the magnetic anisotropy, associated with the transverse part of the exchange interaction $J(S^+ s^- + S^- s^+)$, approximately follows a $D_{\text{eff}} = D_0[1 - \beta(\rho J)^2 + \dots]$ dependence on the exchange coupling (here D_0 is the bare anisotropy, D_{eff} the renormalized value).

In the simple picture, the relative magnitudes of these two channels (YSR and spin-flip) are not constrained and, in principle, both of these effects should be observed simultaneously [35, 36]. Nevertheless, so far no experiment has shown the presence of both at the same time. This suggests that the complete picture of the interplay between these two effects is more complicated, requiring a full many-body treatment of the quantum mechanical spin degree of freedom interacting with a (gapped) continuum of electrons.

Individual MPc molecules on NbSe₂. Figure 1c shows topographic STM images of isolated MPc molecules on NbSe₂ (see Methods for experimental details). Their topographic appearance already reflects differences that allow us to classify them into two groups: The metal ion appears as a protrusion in FePc, CoPc and MnPc and as a depression in CuPc. The different contrast is due to the large respectively small coupling of the out of plane d -orbitals near the Fermi level with the tip states [37].

To characterize the spin states of different MPcs, we recorded the differential conductance spectra (dI/dV curves) with a superconducting tip placed over the center of the molecules, see Fig. 2a. For CoPc and MnPc, there are two peaks that are located at symmetric bias voltages within the superconducting gap. These sub-gap peaks are due to the formation of

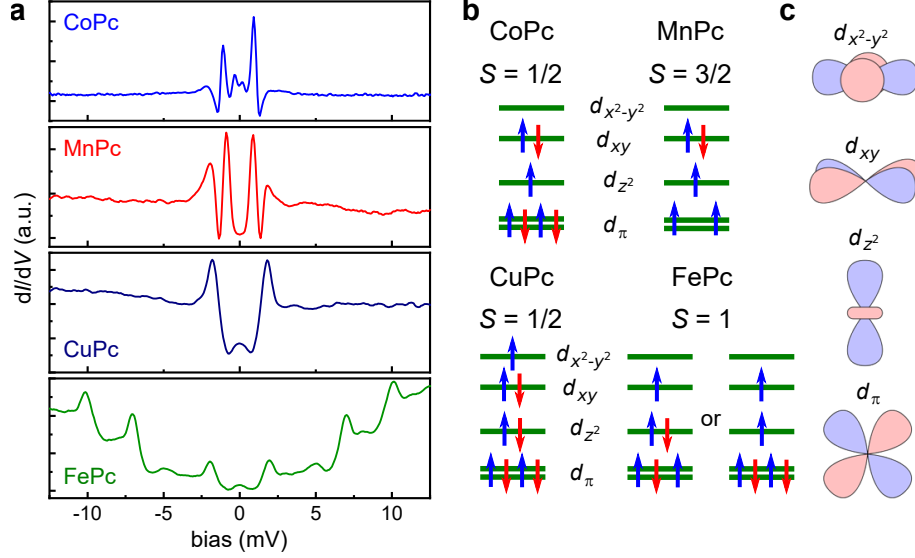


FIG. 2. **Spectra and magnetic states of the different MPc molecules used in this study.** **a**, Differential conductance spectra (dI/dV) recorded over the center of the different MPcs with a superconducting tip. **b**, The ground state spin configurations of the different MPcs. For FePc, we show two possible spin configurations (having similar energy). **c**, Illustration of the different d -orbital symmetries.

YSR states and indicate a sizable magnetic interaction with the superconducting substrate caused by an unpaired spin in the d_{z^2} -orbital (see Fig. 2b for the spin states of the molecules). This orbital is subject to strong coupling with the electronic states of the substrate due to its symmetry, while the spins on the d_{xy} - and $d_{x^2-y^2}$ -orbitals are instead expected to be only weakly coupled [38]. The dI/dV curve taken on the CuPc molecules shows the unperturbed superconducting gap of NbSe₂ due to the absence of unpaired spin in the d_{z^2} orbital (Fig. 2b). As a $S = 1/2$ system, CuPc is also not expected to show any spin-flip excitations.

While the dI/dV curves taken on FePc molecules do not show any features within the gap, there are remarkable features outside it. Their symmetric appearance indicates that these features result from inelastic excitations [28, 39, 40]. This identification is further confirmed by the fact that their shape is similar in form as the edges of the superconducting band [18]. Interestingly, unlike in the previous studies that required decoupling the magnetic molecules using an extra organic ligand as a spacer [18, 25], we observe these signals already when the molecule is directly adsorbed on the superconducting substrate. Since FePc is also expected to have a dominant d_{z^2} -character, the molecule-substrate interaction should

be similar to CoPc and MnPc. The surprising absence of YSR states on FePc suggests that the magnetic interaction with the superconducting substrate is actually weak, which would be at odds with an unpaired spin occupying a d_{z^2} -orbital. FePc has spin triplet $S = 1$ electronic ground state and DFT calculations suggest that FePc on NbSe₂ has the same spin as in the gas phase (Supplementary Information). Although the exact configuration of the ground state is still under debate [41, 42], two configurations separated by 80 meV have been proposed, see Fig. 2b. The configuration with two electrons on the d_{z^2} -orbital is predicted to have lower energy [41], and the absence of a YSR state in our experiments also suggests that the ground state does not have an unpaired d_{z^2} -electron.

We have verified the spin triplet state of FePc and that the observed transitions do indeed correspond to inelastic spin excitations by acquiring the dI/dV spectra at different strengths of the magnetic field (B) that is applied perpendicular to the sample surface (see Supplementary Information for details). The energies of the first and second feature change with B in a way consistent with a spin-state $S = 1$ with transverse anisotropy. Fitting the data with a phenomenological spin Hamiltonian $H_{\text{eff}} = g\mu_B B S_\gamma + D S_z^2 + E(S_x^2 - S_y^2)$, where g is the Landé g factor, μ_B the Bohr magneton and S_γ the spin component along the field direction, we obtain $D = 5.5$ meV and $E = 1.4$ meV indicating easy-plane magnetic anisotropy. The positive value of D is comparable to the bulk value (in contrast to the measurements on oxidized Cu(110) surface giving $D < 0$) [42, 43].

Tuning the exchange coupling with the substrate. The exchange coupling between the magnetic impurity and the substrate can be modulated by changing the adsorption site of the molecule [3, 44]. We successfully positioned CoPc and FePc molecules on different adsorption sites through STM manipulation (see Supplementary Information Fig. S3). Interestingly, the energy positions of both the YSR states and the inelastic features change as the adsorption site is altered. On CoPC, the YSR states can even change between particle- or hole-like character depending on the adsorption site, similarly to the reported results on MnPc adsorbed on Pb(111) [23]. On FePc, adsorption site causes variations of both E and D with typical values in the range of 1.2 – 2.7 meV and 4.2 – 9.0 meV, respectively.

The sensitivity of the YSR states and spin-excitations to small variations in the adsorption configuration suggests that they could be tuned continuously by the force exerted by the STM tip. Figure 3 shows a series of tunneling spectra measured at different tip-sample distances above the central ion of the MPc molecule. We start all the experiments at a

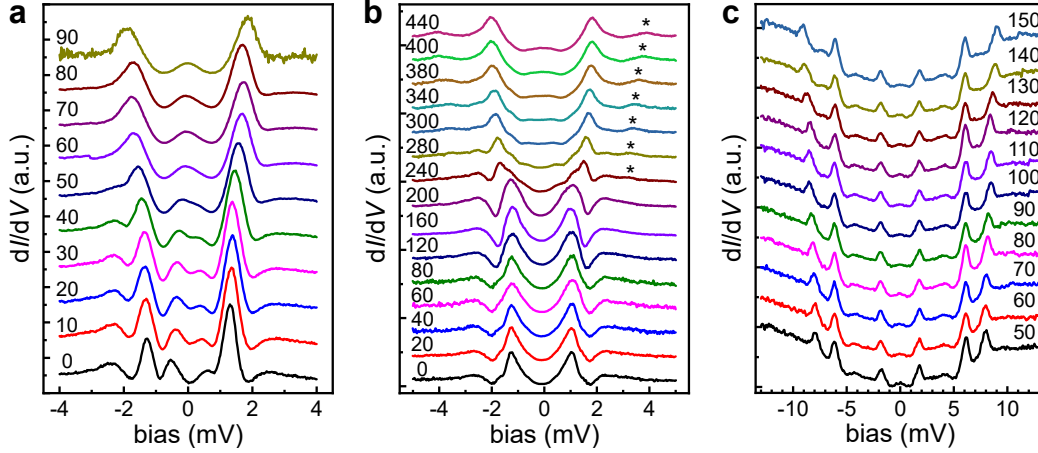


FIG. 3. **Reversible spectral evolution on MPcs.** **a,b,c**, Normalized dI/dV spectra recorded over CoPc (**a**), MnPc (**b**), and FePc (**c**) at different tip-sample distances from far (bottom) to close (top). Starting from the tip-sample distance determined by the set-point conditions, the tip is approached by a distance of z_{offset} indicated in the figure (values in pm).

distance determined by the set-point conditions and approach the tip by a distance of z_{offset} before recording the spectrum. The dI/dV spectra on a CoPc molecule, Fig. 3a, show a shift of the YSR resonances towards higher bias. At $z_{\text{offset}} \approx 60$ pm, the YSR resonances have merged with the superconducting coherence peaks at the gap edge. The dI/dV spectra on MnPc measured under similar conditions, Fig. 3b, also show a clear shift of the YSR resonance towards the superconducting gap edge. Moreover, at around $z_{\text{offset}} = 240$ pm, as the YSR resonance is merging with the superconducting coherence peak, a new symmetric pair of peaks is emerging outside the gap (marked with *). Finally, in FePc, Fig. 3c, the two spin excitation energies monotonously increase with decreasing tip-sample distance.

These variations in the YSR and spin excitations states of the MPc molecules on NbSe₂ surface can be understood considering the force induced by the proximity of the STM tip to the molecules [26, 27, 45]. Under this force, the metal ion is expected to be pulled towards the STM tip. This has the largest effect on the out-of-plane d -orbitals ($d_{xz/yz}$ and d_{z^2}), where the overlap with the substrate wave function will be strongly affected.

In the case of the $S = 1/2$ molecule CoPc, the force affects the exchange coupling strength J between the local spin and the Cooper pairs in NbSe₂ by pulling the impurity towards the tip. This reduces the coupling between the d_{z^2} -orbital and the NbSe₂ and the YSR states move to the SC coherence peaks (J decreases) (Fig. 3a). In the case of $S = 1$ FePc

(Fig. 3c), the effect of the tip-sample force results in a monotonous increase of both spin excitation energies. In addition to modifying the exchange coupling J with the substrate by reducing the hybridisation, the presence of the tip might also affect the energies of the d -orbitals slightly. This causes the bare magnetic anisotropy D_0 , which is an admixture of low-lying excited states of the molecules [46], to be directly affected by the tip-sample distance. In this system, it is not possible to distinguish whether the effective anisotropy D_{eff} changes dominantly through the variation of D_0 or J .

In MnPc ($S = 3/2$), the coupling strength J decreases as the tip-sample distance decreases, which leads to the migration of the YSR states towards the superconducting gap edge and the recovery of the superconducting coherence peaks. When YSR are close to the gap edges, the spectra also show new features outside the gap that are symmetric with respect to zero bias, which are due to spin-flip excitations. In MnPc, the only possible spin-excitation is between $M_s = \pm 1/2$ and $M_s = \pm 3/2$ levels, which are separated in energy by $2D$ in the presence of axial magnetic anisotropy. Subtracting the value of the tip superconducting gap yields an axial anisotropy parameter of $D \approx 0.7$ meV, which is close to the bulk value [47] (see below for more detailed analysis).

Within the conventional picture of the formation of YSR states and the spin-flip excitations, where the quantum fluctuations are neglected, there is no reason to expect a cross-over behaviour from the YSR states to spin-excitations. These conduction channels should be independent and readily observable at the same time. To resolve this disagreement with our experimental results, we need to go beyond the simple theory and consider the full effect of the substrate on the impurity spin.

Full microscopic model and comparison with experiment. The magnetic impurity is described by a multi-orbital Anderson model for the relevant d -shell orbitals [48], which can be reduced in a given charge state to an effective model that takes the form of a Kondo Hamiltonian with the spin degree of freedom, S , only [49, 50] (see Methods and Supplementary Information for details). Since the total spin operator has contributions from all d -orbitals, it is in general exchange coupled to different symmetry-adapted combinations of states from the substrate with different values of Kondo coupling strength, J_i . These differences are due to the unequal orbital energies and hybridization strengths. Only those J_i that are sufficiently large need to be retained; in the problems considered here, a single orbital is always strongly dominant, as evidenced by the presence of a single pair of sub-gap

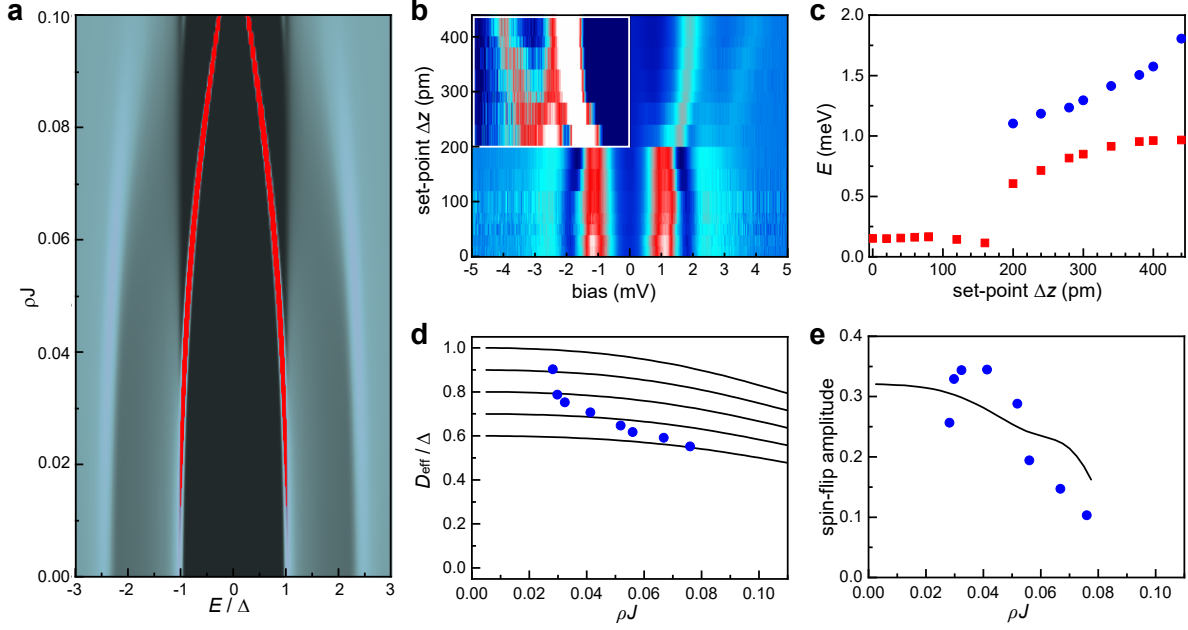


FIG. 4. **Competition between YSR states and spin-flip excitations in spectroscopy of MnPc molecules.** **a**, Theoretical spectral functions for a magnetic impurity ($S = 3/2$) on a superconductor with varying exchange coupling J (spectra normalized by the value at high energy). **b**, Colour-scale plot of the measured tunneling conductance as a function of the tip-sample distance (area inside the white rectangle is shown in enhanced contrast). **c**, Extracted energies of the YSR resonances (red squares) and the spin-flip excitations (blue circles). **d**, Comparison between the experimental D_{eff} (symbols) and the calculated values (solid lines with $D_0/\Delta = 0.6 - 1.0$) scaled by the superconducting gap Δ as a function of the exchange coupling with the substrate. **e**, Extracted experimental values (blue circles) and calculation results (black line) of the amplitude of the spin-flip transition as a function of the exchange coupling with the substrate.

YSR peaks. In the model we also take into account the spin-orbit coupling that leads through orbital excitations to residual magnetic-anisotropy terms. We solve the resulting single-channel anisotropic Kondo model with high spin S using the numerical renormalization group (NRG) method. This method provides a numerically exact solution to this problem.

Figure 4a shows the calculated spectral functions as a function of the exchange coupling between the magnetic impurity and the superconductor for an impurity with $S = 3/2$, as relevant for MnPc. In the absence of anisotropy ($D = E = 0$), the binding of a Bogoliubov quasiparticle would lead to an emergence of a YSR bound state with the spin reduced by

1/2 (YSR screening from $S = 3/2$ to $S = 1$), giving rise to a single pair of YSR peaks. The phenomenology in the isotropic case is similar to that in the classical model, where the impurity is described as a static local magnetic field that binds Bogoliubov quasiparticles of the opposite spin direction. The many-body character of the sub-gap states is, however, revealed in the presence of magnetic anisotropy, which leads to the splitting of the sub-gap $S = 1$ multiplet into the low-energy $|S_z = 0\rangle$ state and the high-energy $(1/2)(|S_z = 1\rangle \pm |S_z = -1\rangle)$ states [51]. For $D \ll \Delta$, such splitting is directly observable [23]. When the anisotropy is large, as is the case here, the high-energy states are pushed instead into the continuum and only the $|S_z = 0\rangle$ sub-gap state is observable. Furthermore, one finds additional features outside the gap that are related to the transitions within the unscreened $S = 3/2$ multiplet [18]. These spectral steps correspond to the spin-flip excitations, similar to the those in systems with normal-state substrates [30, 52]. The exchange coupling to the substrate determines the energy shift as well as the lifetime broadening of the excited states [18, 34]. NbSe₂ is a soft-gap superconductor with a small but finite concentration of sub-gap states, hence the excited spin states have even for $\omega_{sf} = 2D < 2\Delta$ relatively short lifetimes compared to hard-gap superconductors, because the dominant decay channel (emission of particle-hole excitations) is here open. For this reason, a finite value of J leads to significant broadening of the spin-flip excitations. Considering the required magnitude of J for the YSR states to be visibly separated from the gap edges, it is unlikely to be able to experimentally well resolve both spectral features at a given value of the exchange coupling.

The theory curves in Fig. 4a can be compared with the experimental results shown in Fig. 4b. At small values of $z_{\text{offset}} < 200$ pm, only the YSR resonances are visible. As the tip is approached further, the YSR peaks merge with superconducting gap edges and spin-flip features emerge at bias voltage between 3 and 4 mV. The energies of the YSR peaks and spin-flip excitations are shown in Fig. 4c (the superconducting gap of the tip has been subtracted). We can estimate the exchange coupling with the substrate by comparing the theoretical and experimental YSR energies (see Supplementary Figure S7). This allows plotting the renormalized (effective) magnetic anisotropy D_{eff} and the intensity of the spin-flip transitions as a function of the estimated exchange coupling as shown in Figs. 4d,e. Such a calibration is possible because the energy of the YSR state is found to depend only very weakly on the precise value of D in the experimentally relevant interval of parameter values (Supplementary Fig. S7). The comparison with theoretical results (solid lines in

Fig. 4d) yields a value of $D_0/\Delta \sim 0.7$ for the non-renormalized (bare) value of the magnetic anisotropy. The experimental values actually deviate from the theoretical trend expected for a fixed value of D_0 . This is the case for all couplings J , but more particularly for small J , which corresponds to the largest tip-molecule interaction in the experiment. It is likely that the interaction with the tip distorts the molecular geometry or induced charge transfer with the metal ion resulting in a change in the bare value of D itself. The presence of the YSR resonances thus allows us to disentangle the two contributions to the variation of D_{eff} . The extracted value D_0 as a function of the tip-sample distance is plotted in Supplementary Fig. S8.

The intensity of the spin-flip transition is plotted in Fig. 4e, where we observe a monotonous decrease with increasing J (except the first two points, where the reason is again likely to be the tip-molecule interaction). The value at low J is close to the theoretically expected value of 0.4 for pure spin-slip excitations on a normal metal substrate (see Fig. S9 for details) [32, 33]. The experimental values can be compared to the theoretical predictions (solid line) again highlighting the strong correspondence between theory and experiments. Details on extracting the visibility of the spin-slip transitions from computed spectral functions are given in the Supplementary Information.

Conclusions. We have experimentally and theoretically investigated the spectral evolution in different metal phthalocyanine molecules as a function of the exchange coupling between the magnetic impurity and the superconducting substrate. In the case of MnPc, we have demonstrated for the first time the evolution from the YSR states to spin-flip transitions as the coupling is reduced. The spin-flip excitations are broadened and washed out at higher values of the exchange coupling making them difficult to detect experimentally simultaneously with the YSR states. Our results provide fundamental new insight on the behaviour of atomic scale magnetic/superconducting hybrid systems. The detailed understanding of these systems is invaluable for the future design and control of atomic scale magnetic systems, including e.g. artificial topological superconductors and spin logic devices.

METHODS

Sample preparation. Sample preparation and subsequent STM experiments were carried out in an ultrahigh vacuum system with a base pressure of $\sim 10^{-10}$ mbar. The $2H$ -NbSe₂ single crystal (HQ Graphene, the Netherlands) was cleaved in situ by attaching a tape to the crystal surface and pulling the tape in vacuum in the load-lock chamber using the sample manipulator. MPc molecules (Sigma-Aldrich) were deposited from an effusion cell held at 390°C onto a freshly cleaved NbSe₂ at room temperature.

STM measurements. After the MPc deposition, the sample was inserted into the low-temperature STM (Unisoku USM-1300) and all subsequent experiments were performed at $T = 4.2$ K. STM images were taken in the constant-current mode. dI/dV spectra were recorded by standard lock-in detection while sweeping the sample bias in an open feedback loop configuration, with a peak-to-peak bias modulation of $50 - 100 \mu\text{V}$ at a frequency of 709 Hz. The procedure for acquiring a spectrum was as follows: the tip was moved over the molecule at the imaging parameters (e.g. $V = 0.6$ V and $I = 5$ pA), the tip-sample distance was reduced by changing the setpoint to e.g. 200 pA at 100 mV. Finally, after disconnecting the feedback at the beginning the dI/dV spectrum, the tip-sample distance was decreased by a further $50 - 100$ pm (z_{offset}) to increase the signal to noise ratio. The detailed numbers are given in the figure captions.

The NbSe₂ tip was prepared by indenting the tip into the NbSe₂ surface by a few nanometers while applying a voltage of 10 V. Manipulation of the MPc was carried out by placing the tip above the centre of the molecule with a bias voltage of 0.1 V and the current was increased to 1 nA with the feedback engaged. The tip was then dragged towards the desired location.

DFT calculations. Density functional theory calculations were performed with the FHI-AIMS computational package [53, 54] and the PBE generalized gradient approximation for the exchange-correlation functional [55]. We used the standard "light" numerical settings and basis sets of numeric atomic-centered orbitals tested and recommended by FHI-AIMS. Periodic NbSe₂ supercells were sampled with a 2×2 k -point grid centred on the Γ point. Van der Waals interactions were included by the post-SCF Tkatchenko-Scheffler correction [56]. Before computing the electronic structure, all atomic forces were relaxed to < 0.01 eV/Å.

NRG calculations. The quantum impurity problems were solved with the numerical renormalization group method [57, 58] using the "NRG Ljubljana" implementation. We used the discretization parameter $\Lambda = 2$ with $N_z = 16$ interleaved discretization grids, keeping up to 12000 multiples at each step of the iteration. The spectra were computed using the density-matrix NRG algorithm [59]. The energies of the sub-gap states were extracted directly from the renormalization-group flow diagrams, while the energies of the spin-flip excitations were extracted from the peak position in the transverse component of the dynamical spin susceptibility of the impurity. Further details are provided in the Supplementary Information.

ACKNOWLEDGEMENTS

This research made use of the Aalto Nanomicroscopy Center (Aalto NMC) facilities and was supported by the European Research Council (ERC-2017-AdG no. 788185 "Artificial Designer Materials"), Academy of Finland (Academy Research Fellow no. 256818 and Post-doctoral Researcher nos. 309975 and 316347), and the Aalto University Centre for Quantum Engineering (Aalto CQE). Our DFT calculations were performed using computer resources within the Aalto University School of Science Science-IT project and the Finnish CSC-IT Center for Science. R.Ž. acknowledges the support of the Slovenian Research Agency (ARRS) under P1-0044 and J1-7259.

AUTHOR CONTRIBUTIONS

S.K., T.O. and P.L. conceived and planned the experiment. S.K. performed the measurements. S.K. and P.L. analysed the STM data. R.Ž. and T.O. carried out the theoretical analysis of the system. M.D. carried out the DFT calculations. All authors jointly authored, commented, and corrected the manuscript.

* Email: peter.liljeroth@aalto.fi

- [1] J. Li, W.-D Schneider, R. Berndt, and B. Delley, "Kondo scattering observed at a single magnetic impurity," *Phys. Rev. Lett.* **80**, 2893–2896 (1998).

- [2] V. Madhavan, W. Chen, T. Jamneala, M. F. Crommie, and N. S. Wingreen, “Tunneling into a single magnetic atom: Spectroscopic evidence of the Kondo resonance,” *Science* **280**, 567–569 (1998).
- [3] K. J. Franke, G. Schulze, and J. I. Pascual, “Competition of superconducting phenomena and Kondo screening at the nanoscale,” *Science* **332**, 940 (2011).
- [4] L. Yu, “Bound state in superconductors with paramagnetic impurities,” *Acta Phys. Sin.* **21**, 75 (1965).
- [5] H. Shiba, “Classical spins in superconductors,” *Prog. Theor. Phys.* **40**, 435–451 (1968).
- [6] A. I. Rusinov, “On the theory of gapless superconductivity in alloys containing paramagnetic impurities,” *Sov. Phys. JETP* **29**, 1101–1106 (1969).
- [7] A. Yazdani, B. A. Jones, C. P. Lutz, M. F. Crommie, and D. M. Eigler, “Probing the local effects of magnetic impurities on superconductivity,” *Science* **275**, 1767–1770 (1997).
- [8] B. W. Heinrich, J. I. Pascual, and K. J. Franke, “Single magnetic adsorbates on s-wave superconductors,” *Prog. Surf. Sci.* **93**, 1 – 19 (2018).
- [9] S. Nadj-Perge, I. K. Drozdov, J. Li, H. Chen, S. Jeon, J. Seo, A. H. MacDonald, B. A. Bernevig, and A. Yazdani, “Observation of Majorana fermions in ferromagnetic atomic chains on a superconductor,” *Science* **346**, 602–607 (2014).
- [10] M. Ruby, F. Pientka, Y. Peng, F. von Oppen, B. W. Heinrich, and K. J. Franke, “End states and subgap structure in proximity-coupled chains of magnetic adatoms,” *Phys. Rev. Lett.* **115**, 197204 (2015).
- [11] R. Pawlak, M. Kisiel, J. Klinovaja, T. Meier, S. Kawai, T. Glatzel, D. Loss, and E. Meyer, “Probing atomic structure and Majorana wavefunctions in mono-atomic Fe chains on superconducting Pb surface,” *npj Quantum Inf.* **2**, 16035 (2016).
- [12] S. Kezilebieke, M. Dvorak, T. Ojanen, and P. Liljeroth, “Coupled Yu-Shiba-Rusinov states in molecular dimers on NbSe₂,” *Nano Lett.* **18**, 2311–2315 (2018).
- [13] M. Ruby, B. W. Heinrich, Y. Peng, F. von Oppen, and K. J. Franke, “Exploring a proximity-coupled Co chain on Pb(110) as a possible Majorana platform,” *Nano Lett.* **17**, 4473–4477 (2017).
- [14] G. C. Ménard, S. Guissart, C. Brun, R. T. Leriche, M. Trif, F. Debontridder, D. Demaille, D. Roditchev, P. Simon, and T. Cren, “Two-dimensional topological superconductivity in Pb/Co/Si(111),” *Nat. Commun.* **8**, 2040 (2017).

- [15] M. Ruby, B. W. Heinrich, Y. Peng, F. von Oppen, and K. J. Franke, “Wave-function hybridization in Yu-Shiba-Rusinov dimers,” *Phys. Rev. Lett.* **120**, 156803 (2018).
- [16] H. Kim, A. Palacio-Morales, T. Posske, L. Rózsa, K. Palotás, L. Szunyogh, M. Thorwart, and R. Wiesendanger, “Toward tailoring Majorana bound states in artificially constructed magnetic atom chains on elemental superconductors,” *Science Advances* **4**, eaar5251 (2018).
- [17] S.-H. Ji, T. Zhang, Y.-S. Fu, X. Chen, X.-C. Ma, J. Li, W.-H. Duan, J.-F. Jia, and Q.-K. Xue, “High-resolution scanning tunneling spectroscopy of magnetic impurity induced bound states in the superconducting gap of Pb thin films,” *Phys. Rev. Lett.* **100**, 226801 (2008).
- [18] B. W. Heinrich, L. Braun, J. I. Pascual, and K. J. Franke, “Protection of excited spin states by a superconducting energy gap,” *Nature Phys.* **9**, 765 (2013).
- [19] G. C. Ménard, S. Guissart, C. Brun, S. Pons, V. S. Stolyarov, F. Debontridder, M. V. Leclerc, E. Janod, L. Cario, D. Roditchev, P. Simon, and T. Cren, “Coherent long-range magnetic bound states in a superconductor,” *Nat. Phys.* **11**, 1013–1016 (2015).
- [20] M. Ruby, F. Pientka, Y. Peng, F. von Oppen, B. W. Heinrich, and K. J. Franke, “Tunneling processes into localized subgap states in superconductors,” *Phys. Rev. Lett.* **115**, 087001 (2015).
- [21] M. Ruby, Y. Peng, F. von Oppen, B. W. Heinrich, and K. J. Franke, “Orbital picture of Yu-Shiba-Rusinov multiplets,” *Phys. Rev. Lett.* **117**, 186801 (2016).
- [22] L. Cornils, A. Kamlapure, L. Zhou, S. Pradhan, A. A. Khajetoorians, J. Fransson, J. Wiebe, and R. Wiesendanger, “Spin-resolved spectroscopy of the Yu-Shiba-Rusinov states of individual atoms,” *Phys. Rev. Lett.* **119**, 197002 (2017).
- [23] N. Hatter, B. W. Heinrich, M. Ruby, J. I. Pascual, and K. J. Franke, “Magnetic anisotropy in Shiba bound states across a quantum phase transition,” *Nat. Commun.* **6**, 8988 (2015).
- [24] N. Hatter, B. W. Heinrich, D. Rolf, and K. J. Franke, “Scaling of Yu-Shiba-Rusinov energies in the weak-coupling Kondo regime,” *Nat. Commun.* **8**, 2016 (2017).
- [25] B. W. Heinrich, L. Braun, J. I. Pascual, and K. J. Franke, “Tuning the magnetic anisotropy of single molecules,” *Nano Lett.* **15**, 4024–4028 (2015).
- [26] L. Farinacci, G. Ahmadi, G. Reecht, M. Ruby, N. Bogdanoff, O. Peters, B. W. Heinrich, F. von Oppen, and K. J. Franke, “Tuning the coupling of an individual magnetic impurity to a superconductor: Quantum phase transition and transport,” *Phys. Rev. Lett.* **121**, 196803 (2018).

- [27] L. Malavolti, M. Briganti, M. Hänze, G. Serrano, I. Cimatti, G. McMurtrie, E. Otero, P. Ohresser, F. Totti, M. Mannini, R. Sessoli, and S. Loth, “Tunable spinsuperconductor coupling of spin 1/2 vanadyl phthalocyanine molecules,” *Nano Lett.*, ASAP article (2018).
- [28] A. J. Heinrich, J. A. Gupta, C. P. Lutz, and D. M. Eigler, “Single-atom spin-flip spectroscopy,” *Science* **306**, 466 (2004).
- [29] C. F. Hirjibehedin, C .P. Lutz, and A. J. Heinrich, “Spin coupling in engineered atomic structures,” *Science* **312**, 1021 (2006).
- [30] C. F. Hirjibehedin, C.-Y. Lin, A. F. Otte, M. Ternes, C .P. Lutz, B. A. Jones, and A. J. Heinrich, “Large magnetic anisotropy of a single atomic spin embedded in a surface molecular network,” *Science* **317**, 1199 (2007).
- [31] R. Wiesendanger, “Spin mapping at the nanoscale and atomic scale,” *Rev. Mod. Phys.* **81**, 1495–1550 (2009).
- [32] M. Ternes, “Spin excitations and correlations in scanning tunneling spectroscopy,” *New J. Phys.* **17**, 063016 (2015).
- [33] M. Ternes, “Probing magnetic excitations and correlations in single and coupled spin systems with scanning tunneling spectroscopy,” *Prog. Surf. Sci.* **92**, 83 – 115 (2017).
- [34] J. C. Oberg, M. R. Calvo, F. Delgado, M. Moro-Lagares, D. Serrate, D. Jacob, J. Fernández-Rossier, and C .F. Hirjibehedin, “Control of single-spin magnetic anisotropy by exchange coupling,” *Nat. Nanotechnol.* **9**, 64 (2013).
- [35] P. Berggren and J. Fransson, “Spin inelastic electron tunneling spectroscopy on local magnetic moment embedded in Josephson junction,” *EPL* **108**, 67009 (2014).
- [36] P. Berggren and J. Fransson, “Theory of spin inelastic tunneling spectroscopy for superconductor-superconductor and superconductor-metal junctions,” *Phys. Rev. B* **91**, 205438 (2015).
- [37] Xi. Lu, K. W. Hipps, X. D. Wang, and U. Mazur, “Scanning tunneling microscopy of metal phthalocyanines: d7 and d9 cases,” *J. Am. Chem. Soc.* **118**, 7197–7202 (1996).
- [38] J. Kügel, M. Karolak, J. Senkpiel, P.-J. Hsu, G. Sangiovanni, and M. Bode, “Relevance of hybridization and filling of 3d orbitals for the Kondo effect in transition metal phthalocyanines,” *Nano Lett.* **14**, 3895–3902 (2014).
- [39] R. C. Jaklevic and J. Lambe, “Molecular vibration spectra by electron tunneling,” *Phys. Rev. Lett.* **17**, 1139–1140 (1966).

- [40] B. C. Stipe, M. A. Rezaei, and W. Ho, “Single-molecule vibrational spectroscopy and microscopy,” *Science* **280**, 1732 (1998).
- [41] J. Fernández-Rodríguez and M. Toby, B. and van Veenendaal, “Mixed configuration ground state in iron(ii) phthalocyanine,” *Phys. Rev. B* **91**, 214427 (2015).
- [42] N. Tsukahara, M. Kawai, and N. Takagi, “Impact of reduced symmetry on magnetic anisotropy of a single iron phthalocyanine molecule on a Cu substrate,” *J. Chem. Phys.* **144**, 044701 (2016).
- [43] N. Tsukahara, K.-i. Noto, M. Ohara, S. Shiraki, N. Takagi, Y. Takata, J. Miyawaki, M. Taguchi, A. Chainani, S. Shin, and M. Kawai, “Adsorption-induced switching of magnetic anisotropy in a single iron(ii) phthalocyanine molecule on an oxidized Cu(110) surface,” *Phys. Rev. Lett.* **102**, 167203 (2009).
- [44] J. Bauer, J. I. Pascual, and K. J. Franke, “Microscopic resolution of the interplay of kondo screening and superconducting pairing: Mn-phthalocyanine molecules adsorbed on superconducting Pb(111),” *Phys. Rev. B* **87**, 075125 (2013).
- [45] M. Ternes, C. González, C. P. Lutz, P. Hapala, F. J. Giessibl, P. Jelínek, and A. J. Heinrich, “Interplay of conductance, force, and structural change in metallic point contacts,” *Phys. Rev. Lett.* **106**, 016802 (2011).
- [46] D.-s. Wang, R. Wu, and A. J. Freeman, “First-principles theory of surface magnetocrystalline anisotropy and the diatomic-pair model,” *Phys. Rev. B* **47**, 14932–14947 (1993).
- [47] C. G. Barraclough, A. K. Gregson, and S. Mitra, “Interpretation of the magnetic properties of manganese (II) phthalocyanine,” *J. Chem. Phys.* **60**, 962–968 (1974).
- [48] A. Georges, L. de’ Medici, and J. Mravlje, “Strong correlations from Hund’s coupling,” *Annu. Rev. Condens. Matter Phys.* **4**, 137–178 (2013).
- [49] A. Horvat, R. Žitko, and J. Mravlje, “Low-energy physics of three-orbital impurity model with Kanamori interaction,” *Phys. Rev. B* **94**, 165140 (2016).
- [50] A. Horvat, R. Žitko, and J. Mravlje, “Spin-orbit coupling in three-orbital Kanamori impurity model and its relevance for transition-metal oxides,” *Phys. Rev. B* **96**, 085122 (2017).
- [51] R. Žitko, O. Bodensiek, and T. Pruschke, “Effects of magnetic anisotropy on the subgap excitations induced by quantum impurities in a superconducting host,” *Phys. Rev. B* **83**, 054512 (2011).

- [52] A. F. Otte, M. Ternes, K. von Bergmann, S. Loth, H. Brune, C. P. Lutz, C. F. Hirjibehedin, and A. J. Heinrich, “The role of magnetic anisotropy in the Kondo effect,” *Nat. Phys.* **4**, 847–850.
- [53] V. Blum, R. Gehrke, F. Hanke, P. Havu, V. Havu, X. Ren, K. Reuter, and M. Scheffler, “Ab initio molecular simulations with numeric atom-centered orbitals,” *Comput. Phys. Commun.* **180**, 2175 – 2196 (2009).
- [54] V. Havu, V. Blum, P. Havu, and M. Scheffler, “Efficient integration for all-electron electronic structure calculation using numeric basis functions,” *J. Comput. Phys.* **228**, 8367 – 8379 (2009).
- [55] J. P. Perdew, K. Burke, and M. Ernzerhof, “Generalized gradient approximation made simple,” *Phys. Rev. Lett.* **77**, 3865–3868 (1996).
- [56] A. Tkatchenko and M. Scheffler, “Accurate molecular van der Waals interactions from ground-state electron density and free-atom reference data,” *Phys. Rev. Lett.* **102**, 073005 (2009).
- [57] K. G. Wilson, “The renormalization group: Critical phenomena and the Kondo problem,” *Rev. Mod. Phys.* **47**, 773–840 (1975).
- [58] R. Bulla, T. A. Costi, and T. Pruschke, “Numerical renormalization group method for quantum impurity systems,” *Rev. Mod. Phys.* **80**, 395–450 (2008).
- [59] W. Hofstetter, “Generalized numerical renormalization group for dynamical quantities,” *Phys. Rev. Lett.* **85**, 1508–1511 (2000).

SUPPLEMENTARY INFORMATION

GEOMETRIES AND SPIN DENSITIES FROM DFT CALCULATIONS

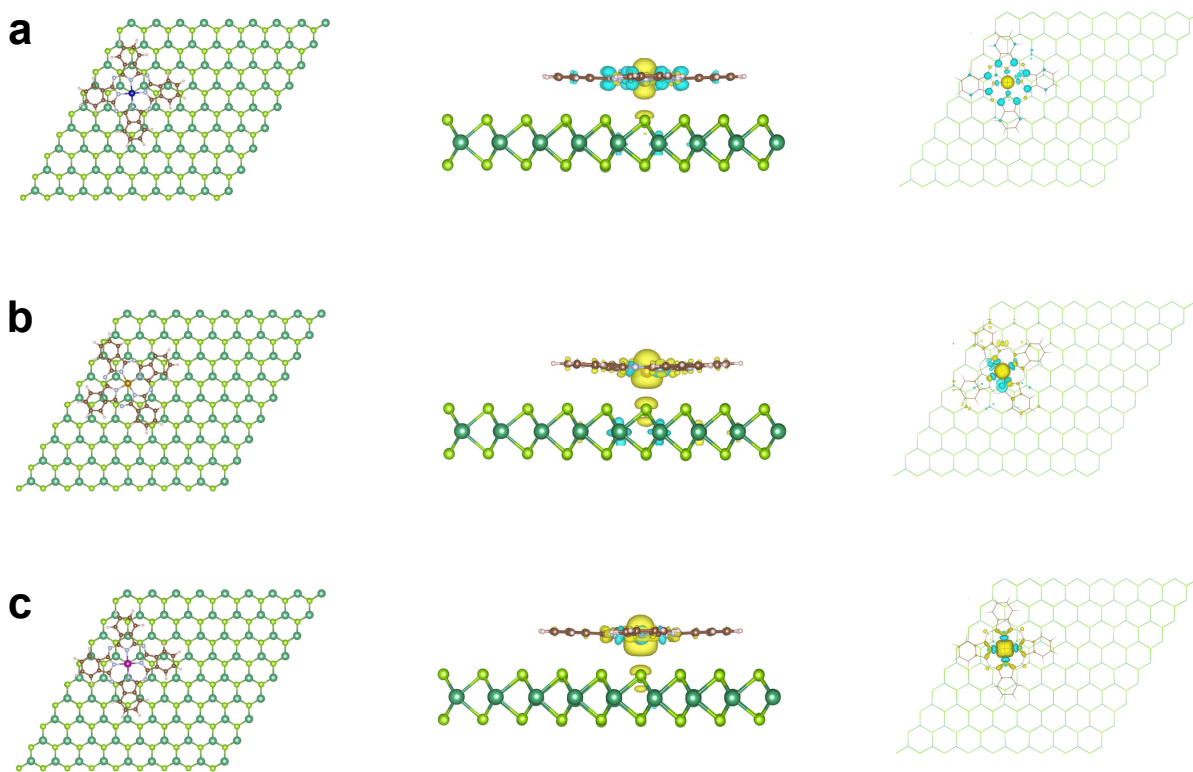


FIG. S1. **Optimized geometries and spin densities.** **a,b,c**, Results for CoPc (a), FePc (b), and MnPc (c) computed with density functional theory (DFT) [53, 54]. The total computed spins for the systems are $S = 0.41$, $S = 1.22$, and $S = 1.72$, respectively. The localized metal atom-projected (Co, Fe, or Mn) spins are $S = 0.49$, $S = 1.10$, and $S = 1.70$, respectively. The localized atom-projected spins differ by < 0.1 compared to their gas phase counterparts with the same DFT parameters and numerical settings.

EXPERIMENTS ON FEPC IN EXTERNAL MAGNETIC FIELD

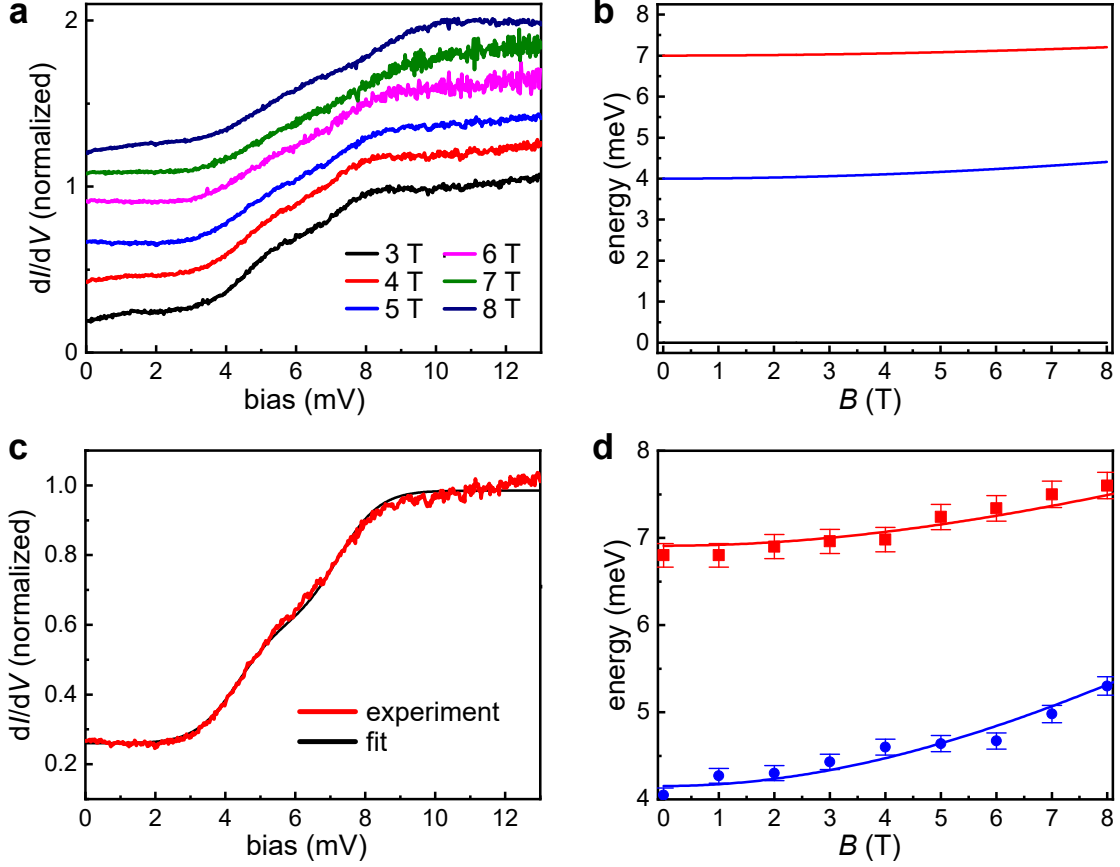


FIG. S2. **Spin-flip excitations in FePc under external magnetic field.** **a**, dI/dV spectra of FePc taken as a function of B_z (3 - 8 T, perpendicular to the sample surface). Each spectrum was acquired directly above the central Fe atom of the FePc. The spectra are vertically offset for clarity (set-point conditions: 20 mV / 1 nA). **b**, Schematic level diagram for an $S = 1$ system with $g = 2$, $D = 5$ meV and $E = 1$ meV. Due to the selection rule $m_S = \pm 1$, there are two allowed transitions from the ground state. **c**, dI/dV spectrum measured under an external field of 5 T showing the splitting of the inelastic spin excitation due to the presence of transverse magnetic anisotropy term E . The black line represents the fit of the spectra [32]. **d**, Spin-flip energies as a function of the external magnetic field. From the fit, we obtain $g = 3.6$, $D = 5.5$ meV, and $E = 1.4$ meV.

We can verify that the observed transitions in FePc do indeed correspond to inelastic spin excitations by acquiring dI/dV spectra at different magnetic (B) field strengths aligned perpendicular to the sample surface. The energies of the first and second feature change

with the external field, demonstrating that these are spin excitations (see Fig. S2). The zero-field splittings (ZFS) are well described by the following spin Hamiltonian:

$$H_{\text{eff}} = DS_z^2 + E(S_x^2 - S_y^2)$$

where D is the axial ZFS constant to determine the magnetic anisotropy, E is the transverse anisotropy, and S_z, S_x, S_y are the spin operators. The selection rule for the spin excitations implies that they can only occur between the states differing by $m_S = \pm 1$. For $S = 1$ spin-state, we would expect only one step in the absence of transverse anisotropy ($E = 0$) and at $B = 0$ T. Transverse anisotropy ($E > 0$) mixes the states and therefore a second step can occur. Hence, the dI/dV spectra on FePc on NbSe₂ suggest spin-state $S = 1$ with transverse anisotropy. We fitted our data using a phenomenological spin Hamiltonian [28, 30, 32, 33]

$$H_{\text{eff}} = g\mu_B BS_\gamma + DS_z^2 + E(S_x^2 - S_y^2)$$

where g is the Landg  g factor, μ_B the Bohr magneton, and S_γ is the component of spin along the direction of the magnetic field. Using the numerical code by M. Ternes [32], we obtain $D = 5.5$ meV, and $E = 1.4$ meV as the best fit with the experimental data. The positive value of D indicates easy plane magnetic anisotropy.

EFFECT OF THE ADSORPTION SITE ON THE YSR STATES AND THE SPIN-FLIP EXCITATIONS

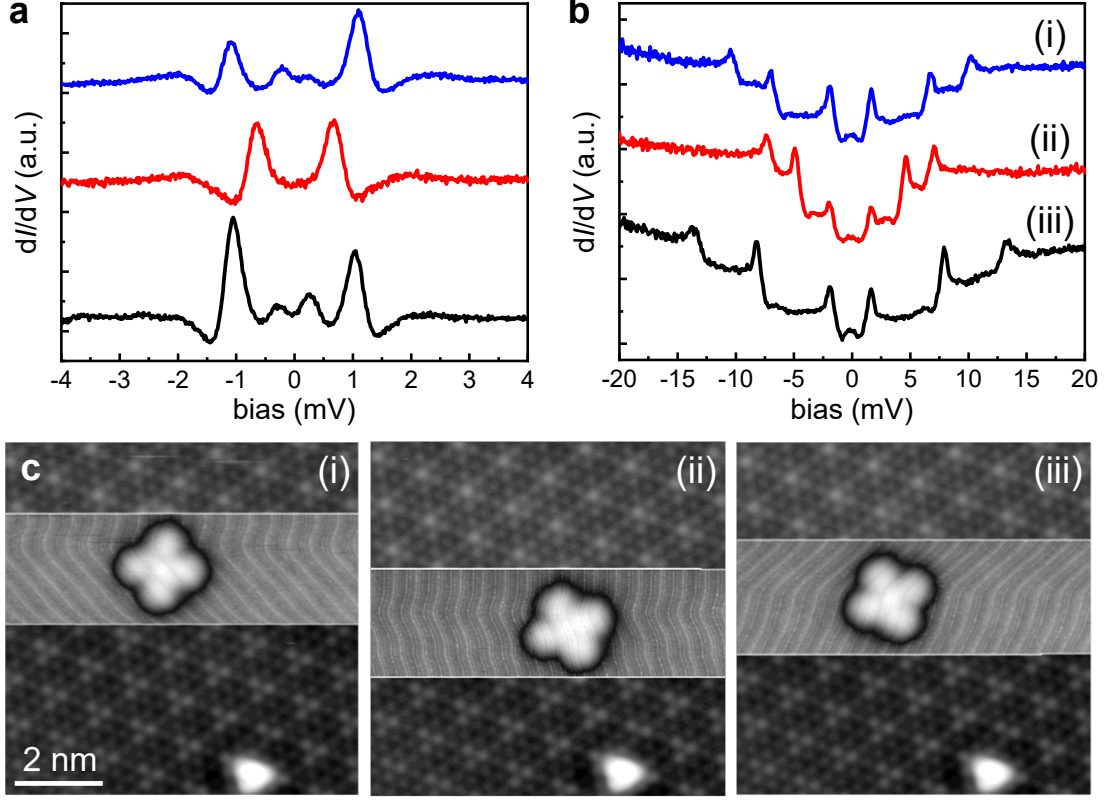


FIG. S3. **Effect of the adsorption site on the YSR states and the spin-flip excitations.** **a**, dI/dV spectra recorded on the same CoPc molecule at different adsorption sites (feedback opened at 10 mV / 1 nA; the spectra are shifted for clarity). All spectra show YSR states inside the superconducting gap. The YSR states change their excitation character between particle- or hole-like depending on the adsorption site of the CoPc molecule on NbSe₂, indicating different signs of the potential scattering term. **b**, dI/dV spectra taken on the same FePc molecule at different adsorption sites (feedback opened at 20 mV / 1 nA; the spectra are shifted for clarity). None of the spectra show any sharp features within the superconducting gap. However, adsorption site causes variations of both E and D with typical values in the range of 1.2 – 2.7 meV and 4.2 – 9.0 meV, respectively. **c**, Determination of the adsorption site corresponding to the three spectra shown in panel b on FePc.

NUMERICAL RENORMALIZATION GROUP CALCULATIONS

The impurity model is solved using the numerical renormalization group (NRG) method [57]. The NRG is a numerical procedure for solving quantum impurity models that is based on a logarithmic discretization of the continuum of electrons (here itinerant electrons from the substrate hybridized with the molecular states). The discretization is controlled by the parameter $\Lambda > 1$ that determines the coarseness of the frequency grid, $\omega_n \sim \Lambda^{-n}$. The discretized Hamiltonian is transformed to a linear tight-binding representation that is diagonalized iteratively. One can compute static properties (expectation values of various operators), thermodynamics, as well as dynamic properties (spectral functions). The results, in particular spectra, can be significantly improved by performing several calculations for interleaved discretizations grids and averaging the results. This tends to remove the discretization artifacts which are periodic functions in $\ln \omega$ with period $\sqrt{\Lambda}$; using $N_z = 2^k$ grids leads to a good cancellation of the fundamental frequency and the first $k-1$ harmonics.

In this work, the calculations have been performed with the “NRG Ljubljana” implementation of the technique. We used $\Lambda = 2$, $N_z = 16$, and kept up to 12000 states/multiplets (or states with energies up to $10\omega_N$, with ω_N the characteristic energy scale at the N -th step of the iteration). The conduction band was assumed to have a constant density of states $\rho = 1/(2\mathcal{D})$ ranging in energy from $-\mathcal{D}$ to \mathcal{D} ; \mathcal{D} also serves as the energy unit. The gap is fixed at $\Delta = 10^{-3}\mathcal{D}$ unless otherwise specified. The spectra were computed using the density-matrix NRG algorithm [59].

The energies of the sub-gap states can be directly extracted from the renormalization-group flow diagrams in the NRG. This approach is significantly more accurate than determining the peak positions in the spectra, and does not suffer from any broadening artifacts. Example results are shown in Fig. S4

The positions of the spin-flip excitation energies can be determined from the spectral function, for instance by locating the peak position or the inflection point that approximately corresponds to the center of the step. Due to strongly changing line-shape of the equilibrium spectral function, this procedure is somewhat ill-defined, and furthermore suffers from possible broadening artifacts. In theoretical calculation using the NRG one can, however, use a more robust and direct approach for very accurately extracting the energies of spin excitations. It consists of computing the transverse part of the dynamical spin

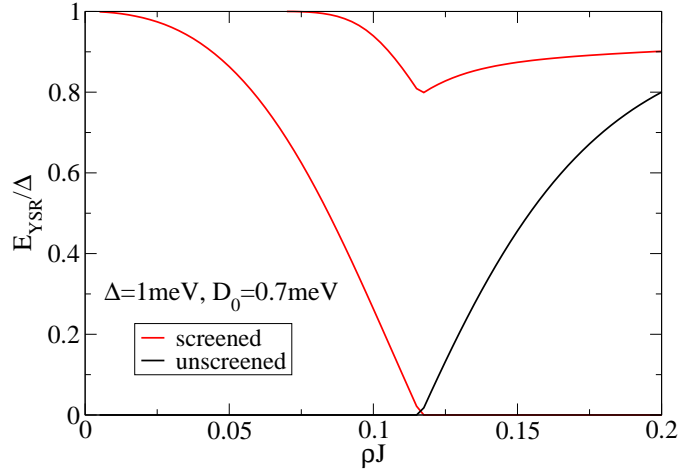


FIG. S4. **Energies of the many-body states, referenced to the ground-state energy of the system.** This diagram shows the energies of all states below the edge of the continuum excitations. The lowest state is hence by definition the ground state, while the excited states give rise to the YSR peaks in the spectra. Black lines correspond to the states resulting from the $S = 3/2$ multiplet after anisotropy splitting (i.e., the $S_z = \pm 1/2$ pair). Red lines correspond to the states resulting from the impurity state “screened” by binding one Bogoliubov quasiparticle from the continuum. These states originate from the $S = 1$ multiplet and are separated into a $S_z = 0$ (lower energy) and a $S_z = \pm 1$ (higher energy) subsets. The $S_z = 0$ YSR state is present for all J , the $S_z = \pm 1$ pair starts emerging from the continuum at $\rho J \approx 0.08$. At $\rho J \approx 0.12$, a quantum phase transition between the $S_z = \pm 1/2$ and $S_z = 0$ many-body states occurs.

susceptibility function

$$\chi_{\perp}(\omega) = \langle\langle S^x; S^x \rangle\rangle_{\omega}. \quad (1)$$

The spin excitation energies can then be directly read off from the peak position, which is unique and very well defined. This is illustrated in Fig. S5

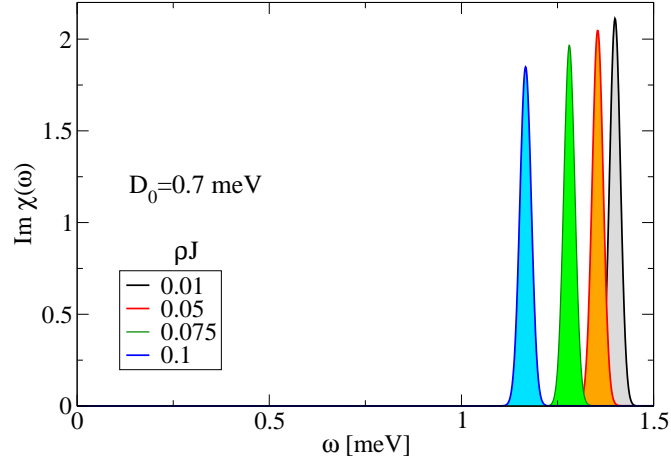


FIG. S5. **Dynamical spin susceptibility for a range of exchange couplings J .** Here we plot the imaginary part of the transverse component of the dynamical spin susceptibility which quantifies the spin-flip transitions of the system. The peak position corresponds to $\omega_{\text{sf}} = 2D_{\text{eff}}$, i.e., the renormalized spin-flip energy. The peak-width is related to the life-time of the spin excitations, but here it is overbroadened for numerical reasons.

PROPERTIES OF THE ANISOTROPIC $S = 3/2$ KONDO MODEL

The spectral functions for a range of values of the exchange coupling for $S = 3/2$ are shown in Fig. S6 (with parameter values corresponding to the experiments on MnPc).

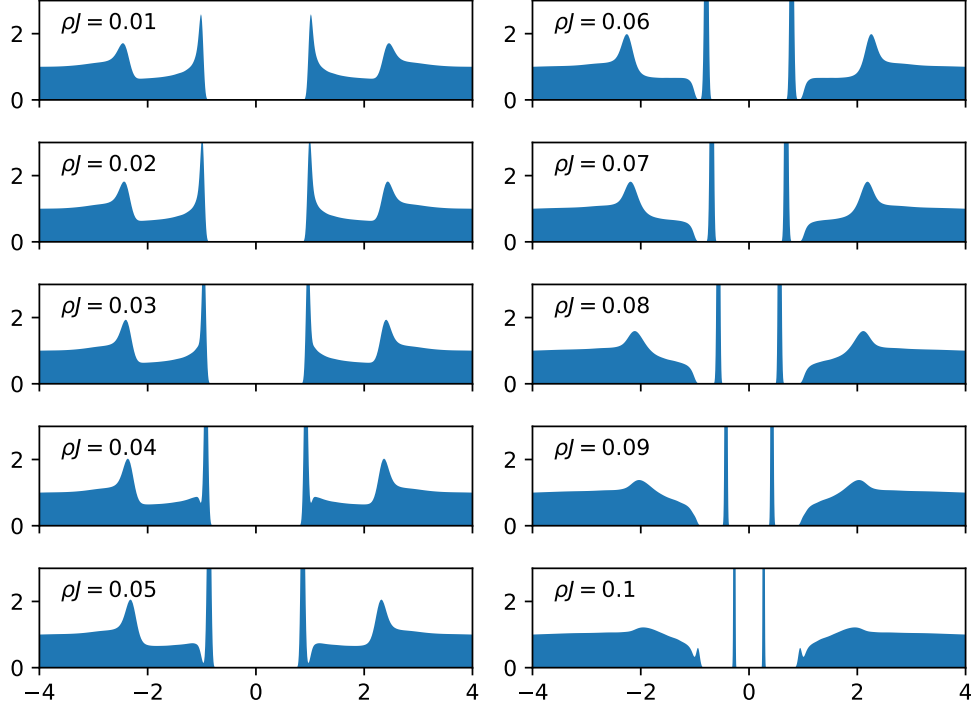


FIG. S6. **Spectral functions for a range of exchange coupling strengths.** These plots correspond to horizontal line-cuts of the density plot in Fig. 4a of the main text. They show more clearly how the YSR state detaches from the band edge of the continuum of Bogoliubov excitations, and how the spin-flip line-shape evolves (in particular for $\rho J \geq 0.06$, i.e., after the emergence of YSR as a well-defined sub-gap state). At $\rho J \sim 0.1$, a new sub-gap feature starts to detach from the band edge: this is an additional YSR state (of type $|S_z = 1\rangle \pm |S_z = -1\rangle$) that results from the magnetic anisotropy splitting of the $S = 1$ YSR multiplet. This parameter range is, however, not experimentally relevant.

The insensitivity of the YSR state energy on D_0 is illustrated in Fig. S7, which enables us to calibrate the exchange coupling based on the experimental YSR energies.

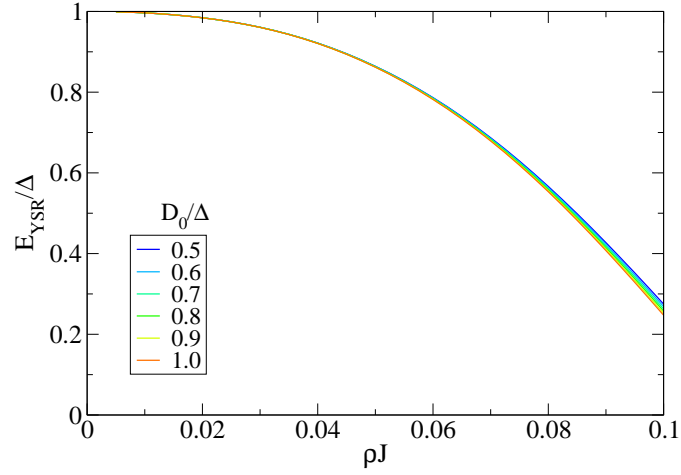


FIG. S7. **Yu-Shiba-Rusinov state energy as a function of exchange J for $S = 3/2$ model.**

The results are extracted from the highly-accurate NRG renormalization flow diagrams. The weak dependence on the value of the bare magnetic anisotropy D_0 enables the use of these results as a calibration of the tip offset above MnPc in terms of the exchange coupling J even in the absence of prior knowledge of the precise value of (bare) anisotropy.

BARE MAGNETIC ANISOTROPY D_0 AS A FUNCTION OF THE TIP-SAMPLE DISTANCE

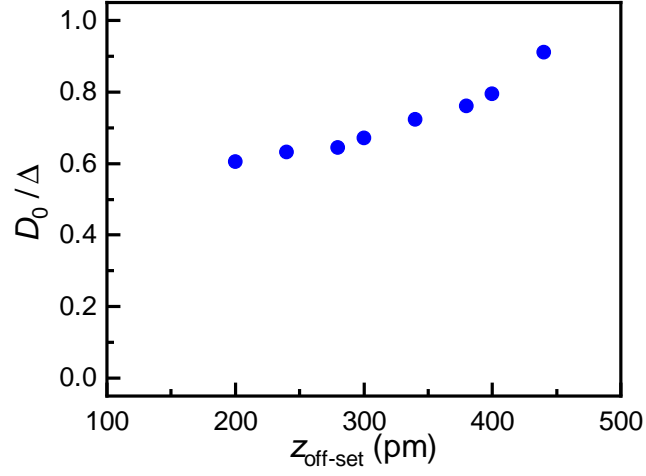


FIG. S8. **Bare magnetic anisotropy D_0 .** These values are extracted from the experimental D_{eff}/Δ values by subtracting the theoretically predicted ρJ dependence and plotted here as a function of the tip-sample distance offset.

COMPARISON OF THE SPECTRAL FUNCTION WITH NORMAL METAL AND SUPERCONDUCTING SUBSTRATE

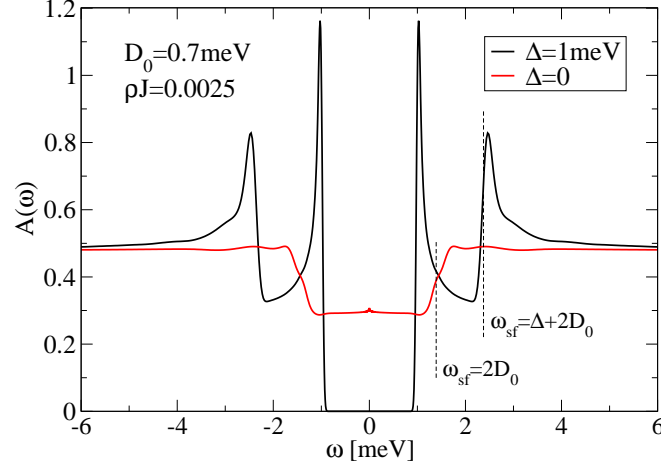


FIG. S9. **Calculated impurity spectral function for normal-state and superconducting substrate.** We compare the low-energy parts of the spectral functions computed for an anisotropic Kondo impurity model ($S = 3/2$, longitudinal anisotropy D_0) in the limit of very small exchange coupling J , so that the Kondo temperature is negligibly small. For normal-state substrate, the spectrum shows steps due to inelastic excitations for bias voltage beyond the spin-flip excitation threshold $\omega_{\text{sf}} = 2D_0$. The significant width of the step is a broadening artifact of the numerical method (lower broadening parameter would lead to stronger artifacts, which are already visible in these results in the form of weak oscillatory features). For superconducting substrate, a gap is formed, while the spin-flip features are shifted to $\omega_{\text{sf}} = \Delta + 2D_0$. Furthermore, the spectral shape of the inelastic excitations inherits the form of the density of states of the superconductor near the threshold of the band of Bogoliubov excitations.

EXTRACTION OF INELASTIC-EXCITATION STEP HEIGHTS

Extracting the amplitude of the inelastic excitations in the case of a normal-state substrate is simple: extract the step amplitude and reference it to the asymptotic value. For a superconducting substrate, the inelastic excitation corresponds to a spectral feature with a complicated shape that also changes with the increasing value of the exchange coupling.

In order to compare these results with the experiments, we have used two different approaches to extract the amplitude from computed spectral functions. For low J (up to $\rho J \approx 0.06$), one can define the height as the difference between the minimum value of LDOS (this point occurs between the edge of the gap and the spin-flip resonance peak) and the asymptotic value. For larger J , this minimum no longer exists. Instead, a plateau-like structure exists for J up to $\rho J \approx 0.09$. In this range, one can define the amplitude as the difference between the value at the center of this plateau and the asymptotic value. Finally, for large J , no meaningful definition exists.

The maximum of the spectral function at the position of the spin excitation does not provide information about the amplitude of the spin-flip excitation, but rather reflects the properties of the bottom edge of the continuum (i.e., for small J , information about the superconducting coherence peak in the impurity spectral function).

The procedure above yields the results shown in Fig. 4e of the main manuscript and corresponds physically to the visibility of the inelastic features. It is in spirit similar to how the spin-flip amplitude can be (and was) estimated experimentally. On the other hand, the true inelastic contribution to the total spectral function can be assessed by comparing the calculated response to that obtained with the same ρJ and large value of D_0 . Example of such curves (at $\rho J = 0.07$) is shown in Fig. S10a. This plot shows the calculated response with $D_0 = 0.7$ meV (black line) and with $D_0 = 5$ meV (red line). The asymptotic value of their difference (blue line) gives direct access to the inelastic contribution to the total spectral function. This is plotted as a function of ρJ in Fig. S10b showing values very close to the expected magnitude of 0.4 for pure spin-flip excitations on a normal metal substrate.

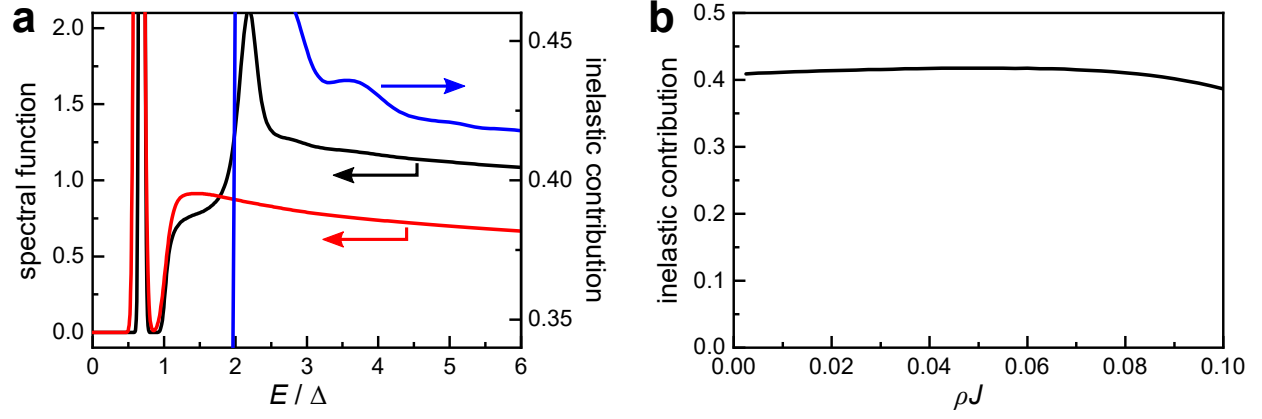


FIG. S10. **Estimating the real inelastic contribution to the total spectral function.** **a**, Calculated spectral functions with $\rho J = 0.07$ and $D_0 = 0.7$ meV (black line) or $D_0 = 5.0$ meV (red line). The difference is given by the blue line. **b**, The asymptotic value of the inelastic contribution as a function ρJ for $D_0 = 0.7$ meV.

PROPERTIES OF THE ANISOTROPIC $S = 1$ KONDO MODEL

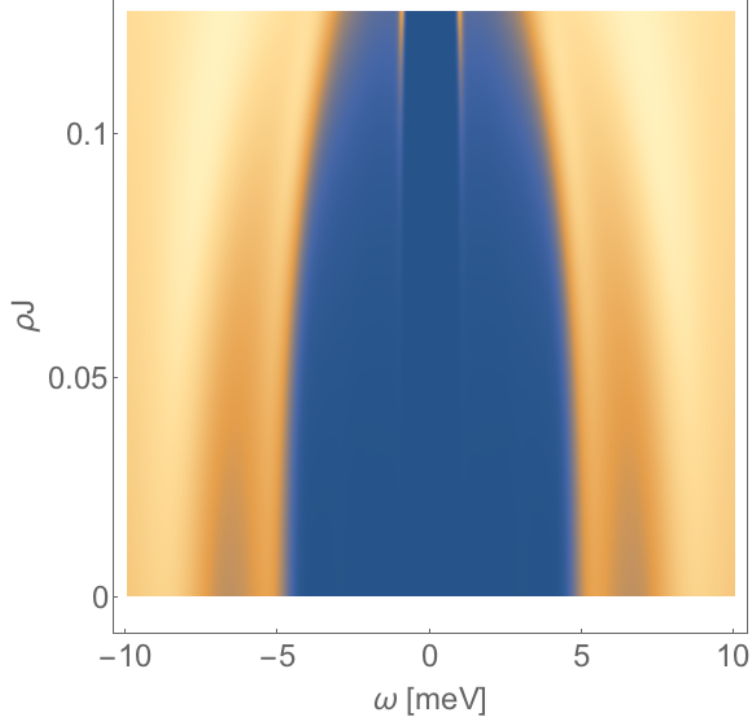


FIG. S11. **Theoretical spectral functions for a $S = 1$ impurity with varying exchange coupling J .** Spectral function for the anisotropic $S = 1$ Kondo impurity with magnetic anisotropy parameters $D = 5.5$ meV and $E = 1.5$ meV (spin-flip excitation energies $D - E = 4$ meV and $D + E = 7$ meV). At low J , the superconducting band edges are hardly visible, but their amplitude increases with increasing J . At still higher J (not shown here), a $S = 1/2$ sub-gap YSR state detaches from the gap edge.